Turkish Journal of Electrical Engineering & Computer Sciences

http://journals.tubitak.gov.tr/elektrik/

Research Article

Turk J Elec Eng & Comp Sci
(2017) 25: 2149 – 2162

doi:10.3906/elk-1602-277

Adaptive sliding mode with time delay control based on convolutions for power flow reference tracking using a VSC-HVDC system

Amar HAMACHE[1,*], Mohand Outaher BENSIDHOUM[1], Hachemi CHEKIREB[2]
[1]Department of Automatics, Faculty of Electrical Engineering and Computer Sciences, Tizi-Ouzou University, Tizi-Ouzou, Algeria
[2]Department of Automatics, National Polytechnic School, Algiers, Algeria

Received: 19.02.2016 • **Accepted/Published Online:** 18.08.2016 • **Final Version:** 29.05.2017

Abstract: This paper deals with the design of an adaptive sliding mode with a time delay control based on convolutions (ASMTDCC) approach for a voltage source converter (VSC) high voltage direct current (HVDC) transmission system for power flow reference tracking over a wide range of operating conditions considering parameter variations and external disturbances. For this purpose, the model of a VSC-HVDC transmission system connecting two asynchronous electrical grids is developed. The problem of designing an ASMTDCC feedback scheme, via a control strategy, is addressed seeking a better performance. For ensuring robust behavior and reducing chattering, the ASMTDCC scheme is realized based on time delay approximation and sliding mode techniques. Theoretical developments and results are illustrated through simulation results.

Key words: High voltage direct current transmission system, power flow, sliding mode control, time delay control, convolution, Lyapunov function

1. Introduction

Explicitly, the most common arguments put forward by the supporters of high voltage direct current (HVDC) rather than high voltage alternative current (HVAC) transmission systems, in addition to the environmental and economical merits are as follows [1–4]: cheaper in long-haul bulk power transmission, asynchronous link, accurate control of power flow both magnitude and direction, fault isolation, and improved link stability.

The HVDC transmission system was proposed with the application of modern electrical transmission systems [5]. Its various capabilities have been discussed in many papers in areas of power flow control [6–8], transient stability improvement, and oscillation damping control [9,10]. Furthermore, in the literature, the HVDC transmission system has been applied in a vast variety of control system investigations, including PI control [11–14], H∞ approach method [15], linearization control [11], sliding mode control [16,17], back-stepping design [18,19], flatness theory-based control [20], and passivity theory-based control [21,22]. All the aforementioned methods, including linear and nonlinear controllers, guarantee asymptotic stability of the closed-loop system. In the literature some intelligent controllers are also proposed [14,17], which have the problem of iteration-based results. Furthermore, the time delay control strategies have demonstrated better robustness and disturbance rejection properties [23–25].

To the best of the authors' knowledge, the ASMTDCC technique for controlling the operation of the VSC-

*Correspondence: hamache81@yahoo.fr

HVDC transmission system, under parameter uncertainties and disturbances, has not been studied according to the literature published so far. Thus, the main contribution of this paper is to verify the dynamic performance of the ASMTDCC as a control solution for the VSC-HVDC transmission system in power flow reference tracking, to meet the inherent uncertain parameters, unmodeled dynamics, and unknown disturbances [16]. The ASMTDCC's capability towards providing a stabilized performance over a wide range of operating conditions and perturbations is discussed.

In line with the above discussion, this paper addresses the problem of ASMTDCC controller design based on the direct Lyapunov stability theory and convolution-based time delay approximation technique for power flow control. The controller is able to track reference signals precisely and is robust against model uncertainties and external disturbances.

The paper is organized as follows: the model of the transmission system is built in section 2. The calculation of current references for AC subsystem is presented in section 3. In section 4, based on Lyapunov theory and convolution-based time delay approximation, the ASMTDCC law is deduced considering the VSC-HVDC AC subsystem dynamics. Section 5 presents simulation results for exhibiting the controller performances and verifying its robustness. Finally, section 6 concludes the paper.

2. Mathematical model of the VSC-HVDC transmission system

This section introduces the state-space model of a VSC-HVDC system established in the synchronous d-q frame, which allows for a decoupled control on the real and the reactive powers, with the high-frequency pulse width modulation (PWM) characteristics of the power electronics. Only the balanced condition is considered in this paper, i.e. the three phases have identical parameters and their voltages and currents have the same amplitude while phase-shifted 120° between themselves.

A typical VSC-HVDC transmission link consists of two converter stations [1,2,11,16]. One station operates as the rectifier station whereas the other operates as the inverter station as shown in Figure 1.

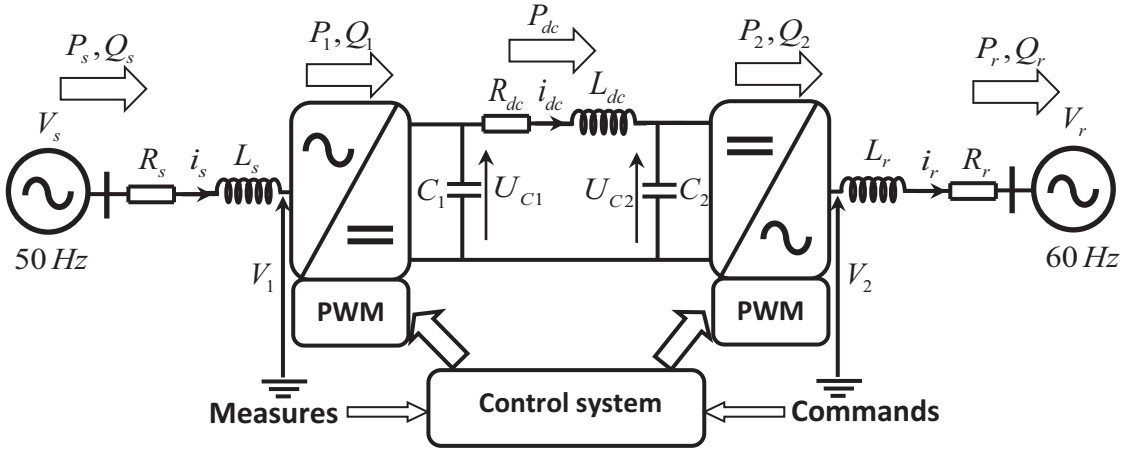

Figure 1. Schematic diagram of the HVDC system.

The real and reactive powers supplied by the sending grid are denoted by P_s and Q_s, respectively, while the corresponding powers entering the receiving grid are P_r and Q_r.

The mathematical model developed in this paper is based upon a rotating $d-q$ frame.

During the transformation of the abc to the $d-q$ frames, a phase-locked loop (PLL) plays a key role. This system is naturally decoupled into two subsystems: the first one is the AC subsystem representing fast dynamics and the second one is the DC subsystem, which represents slow dynamics [16,17].

2.1. AC subsystem

Figure 2 represents the single phase equivalent circuit of the two AC sides of the VSC-HVDC transmission system, which represent the so-called AC subsystem. R_s, L_s, and i_s are the resistance, inductance, and current on the rectifier AC side and R_r, L_r, and i_r are the resistance, inductance, and current on the inverter AC side, respectively. V_1 and V_s are the voltage of the rectifier AC side and the voltage of the sending grid side, respectively. The voltages V_2 and V_r correspond to the inverter AC side and the receiving grid side, respectively.

Figure 2. Single phase equivalent circuit HVDC's AC subsystem.

By applying Kirchhoff's voltage law to the circuits of Figure 2, one can write the following differential equations:

$$L_s \frac{di_{sph}}{dt} + R_s\, i_{sph} = -V_{1ph} + V_{sph} \tag{1}$$

$$L_r \frac{di_{rph}}{dt} + R_r\, i_{rph} = V_{2ph} - V_{rph}, \tag{2}$$

where $ph = a$, b and c is any phase of the three-phase system.

Considering a balanced three-phase system rotating at a pulsation ω_1 and a rotating frame $d_1 - q_1$ initially oriented on angle $\theta_1 = \omega_1 t$, as in Figure 3, the d-q equations of the rectifier side are obtained by transforming equation Eq. (1) using Park's transformation [16] as follows:

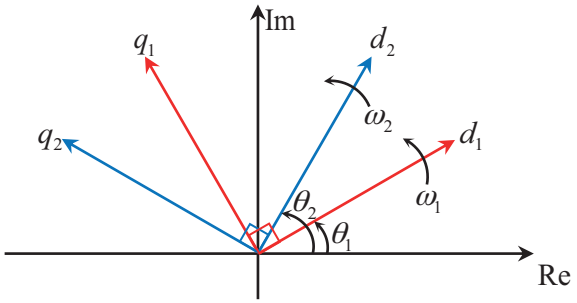

Figure 3. Rotating frames for d-q transformation.

$$\begin{cases} \frac{di_{sd}}{dt} = -\frac{R_s}{L_s} i_{sd} + \omega_1 i_{sq} - \frac{1}{L_s} V_{1d} + \frac{V_{sd}}{L_s} \\ \frac{di_{sq}}{dt} = -\frac{R_s}{L_s} i_{sq} - \omega_1 i_{sd} - \frac{1}{L_s} V_{1q} + \frac{V_{sq}}{L_s} \end{cases} \tag{3}$$

Similarly, the $d-q$ equations of inverter side in a rotating frame at a pulsation ω_2 initially oriented on angle $\theta_2 = \omega_2 t$ are as follows:

$$\begin{cases} \frac{di_{rd}}{dt} = -\frac{R_r}{L_r} i_{rd} + \omega_2 i_{rq} + \frac{1}{L_r} V_{2d} - \frac{V_{rd}}{L_r} \\ \frac{di_{rq}}{dt} = -\frac{R_r}{L_r} i_{rq} - \omega_2 i_{rd} + \frac{1}{L_r} V_{2q} - \frac{V_{rq}}{L_r} \end{cases}, \tag{4}$$

where i_{sd}, i_{sq}, V_{1d}, V_{1q}, V_{sd}, V_{sq} and i_{rd}, i_{rq}, V_{2d}, V_{2q}, V_{rd}, V_{rq} are the $d-q$ axis currents and voltages on the rectifier and inverter AC sides, respectively.

Here ω_1 and ω_2 refer to the pulsations of the rectifier and inverter AC sides, respectively.

The AC subsystem's global mathematical model and state space representation that indicates the relationships among the different system's variables are consequently expressed in the form below:

$$\dot{\mathbf{X}} = \mathbf{A}\,\mathbf{X} + \mathbf{B}\,\mathbf{U} + \mathbf{W}, \tag{5}$$

where $\mathbf{X}$, $\mathbf{U}$, and $\mathbf{W}$ refer, respectively, to the state variables vector, the control signals vector, and the residual terms vector, which represents the $d-q$ components of the system steady state power flow without the VSC-HVDC device, in $d-q$ reference frame.

$$\mathbf{X} = \begin{bmatrix} i_{sd} & i_{sq} & i_{rd} & i_{rq} \end{bmatrix}^T, \quad \mathbf{U} = \begin{bmatrix} V_{1d} & V_{1q} & V_{2d} & V_{2q} \end{bmatrix}^T \text{ and } \mathbf{W} = \begin{bmatrix} \frac{V_{sd}}{L_s} & \frac{V_{sq}}{L_s} & -\frac{V_{rd}}{L_r} & -\frac{V_{rq}}{L_r} \end{bmatrix}^T.$$

The matrices $\mathbf{A}$ and $\mathbf{B}$ are printed out as

$$\mathbf{A} = \begin{bmatrix} -\frac{R_s}{L_s} & \omega_1 & 0 & 0 \\ -\omega_1 & -\frac{R_s}{L_s} & 0 & 0 \\ 0 & 0 & -\frac{R_r}{L_r} & \omega_2 \\ 0 & 0 & -\omega_2 & -\frac{R_r}{L_r} \end{bmatrix} \text{ and } \mathbf{B} = \begin{bmatrix} -\frac{1}{L_s} & 0 & 0 & 0 \\ 0 & -\frac{1}{L_s} & 0 & 0 \\ 0 & 0 & \frac{1}{L_r} & 0 \\ 0 & 0 & 0 & \frac{1}{L_r} \end{bmatrix}.$$

Note that the determinant of $\mathbf{B}$ is given by $\det(\mathbf{B}) = 1 \Big/ (L_s\, L_r)^2 \neq 0$, which means that matrix $\mathbf{B}$ is invertible.

2.2. DC subsystem

Figure 4 represents a schematic diagram of the DC subsystem (DC link), where R_{dc}, L_{dc}, and i_{dc} are its resistance, inductance, and current, respectively [11–18]. P_1 and P_2 refer to real powers on both sides of the converters, as shown in Figure 4.

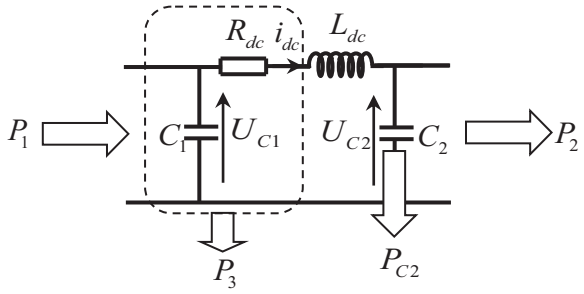

Figure 4. Schematic diagram of the DC link with powers repartition.

P_{C2} refers to the stored power in capacitor C_2 and P_3 represents power losses relative to resistance R_{dc} and capacitor C_1. By applying the principle of real power balance on both sides of the rectifiers, one has

$$P_1 - P_3 - P_{C2} - P_2 = 0 \tag{6}$$

From Eq. (6), P_{C2} can be expressed as

$$P_{C2} = P_1 - P_2 - P_3 \tag{7}$$

If P_{loss} refers to power losses between sending and receiving grid sides, then its expression can be given by

$$P_{loss} = (P_s - P_1) + (P_2 - P_r) + P_3 \tag{8}$$

Using Eq. (7), Eq. (8) can be rewritten as

$$P_{C2} = (P_s - P_r) - P_{loss} \tag{9}$$

The stored power P_{C2} can be replaced in Eq. (8) by its expression Eq. (9) [21],

$$P_{C2} = \frac{C}{2}\frac{dU_{C2}^2}{dt} \tag{10}$$

Thus, the dynamics of inverter side DC square voltage U_{C2}^2 is given as

$$\frac{C}{2}\frac{dU_{C2}^2}{dt} = (P_s - P_r) - P_{loss} \tag{11}$$

In Eq. (11), the term $\Delta P = P_s - P_r$ represents the DC link control and P_{loss} is considered as a disturbance that is assumed to be unknown.

Since the dynamics of the DC link is linear and relatively slow, a conventional PI controller can be used to regulate DC voltage U_{C2} to its rated value U_{C2ref} and reject external disturbances P_{loss} [6–16], as shown in Figure 5.

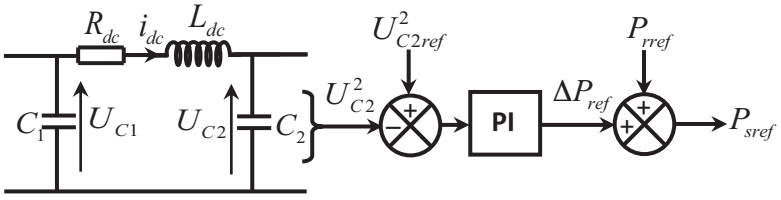

Figure 5. DC voltage control scheme.

3. Control objectives and calculation of current references

After developing the system's mathematical model in state space, a control law formulation is necessary for mainly controlling the active and reactive powers to their set points and governing the DC voltage to its rated value.

The voltage drop and the power losses in the DC link are taken into account with regards to the power flow direction (flow from station 1 to station 2 or vice versa).

The reference values of active and reactive powers supplied to both AC sides of the VSC-HVDC system are given by Eq. (12) [6–16].

$$\begin{cases} P_{sref} = V_{sd}\, i_{sdref} + V_{sq}\, i_{sqref} \\ Q_{sref} = V_{sq}\, i_{sdref} - V_{sd}\, i_{sqref} \\ P_{rref} = V_{rd}\, i_{rdref} + V_{rq}\, i_{rqref} \\ Q_{rref} = V_{rq}\, i_{rdref} - V_{rd}\, i_{rqref} \end{cases} \tag{12}$$

Consequently, with known desired active and reactive power references to be transmitted in the AC receiving line, i_{rdref} and i_{rqref} are obtained as follows:

$$\begin{cases} i_{rdref} = \left(V_{rd}\, P_{rref} + V_{rq}\, Q_{rref}\right) / \left(V_{rd}^2 + V_{rq}^2\right) \\ i_{rqref} = \left(V_{rq}\, P_{rref} - V_{rd}\, Q_{rref}\right) / \left(V_{rd}^2 + V_{rq}^2\right) \end{cases} \tag{13}$$

Similarly to AC receiving line currents, i_{sdref} and i_{sqref} are obtained as follows:

$$\begin{cases} i_{sdref} = \left(V_{sd}\, P_{sref} + V_{sq}\, Q_{sref}\right) / \left(V_{sd}^2 + V_{sq}^2\right) \\ i_{sqref} = \left(V_{sq}\, P_{sref} - V_{sd}\, Q_{sref}\right) / \left(V_{sd}^2 + V_{sq}^2\right) \end{cases} \tag{14}$$

The current references are lumped in the reference state variables vector $\mathbf{X}_{ref} = \left[i_{sdref}\, i_{sqdref}\, i_{rdref}\, i_{rqref}\right]^T$. The calculation of current references vector $\mathbf{X}_{ref}$ in the $d-q$ frame is illustrated in Figure 6.

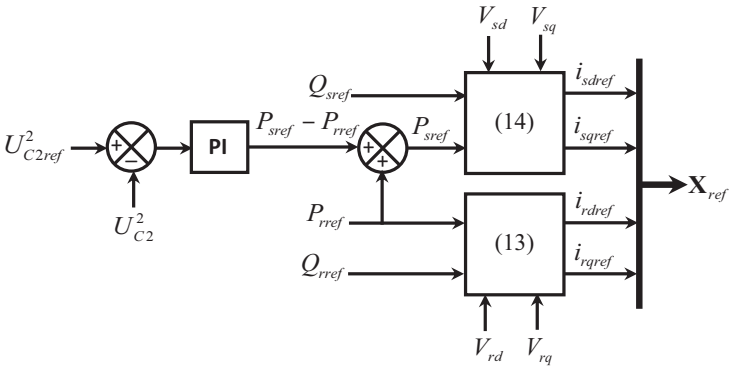

Figure 6. Current references calculation.

4. Designing the ASMTDCC of the VSC-HVDC transmission system

As indicated in section 3, this paper mainly focuses on the inner-loop control of the VSC-HVDC transmission system. In this section a centralized globally asymptotically stabilizing control for the system is presented. We intend to develop a state feedback control that forces the system to track a nonconstant reference current

$\mathbf{X}_{ref}(t)$ in the presence of plant uncertainties and external disturbances that unavoidably affect the state space model Eq. (5) [6–16].

If $\Delta\mathbf{A}$, $\mathbf{\Delta B}$, and $\mathbf{\Delta W}$ are the uncertainties of the system then,

$$\begin{cases} \mathbf{A} = \mathbf{A}_n + \mathbf{\Delta A} \\ \mathbf{B} = \mathbf{B}_n + \mathbf{\Delta B} \\ \mathbf{W} = \mathbf{W}_n + \mathbf{\Delta W} \end{cases}, \tag{15}$$

where subscript 'n' denotes the nominal parts.

If $\mathbf{d}$ is an external disturbance, then all the uncertainties can be lumped as follows:

$$\mathbf{D} = \Delta\mathbf{A}\,\mathbf{X} + \Delta\mathbf{B}\,\mathbf{U} + \Delta\mathbf{W} + \mathbf{d} \tag{16}$$

Let the following reasonable assumptions hold for the system:

1. all the state variables of the system are measurable or estimated,
2. the lumped uncertainty $\mathbf{D}$ is bounded, i.e. there exist four positive upper bounds $\bar{D}_i$ such that

$$|D_i| < \bar{D}_i, \tag{17}$$
$$i = 1\,, ..., 4$$

Using Eqs. (15) and (16), the expression Eq. (5) can be rewritten as

$$\dot{\mathbf{X}} = \mathbf{A}_n\,\mathbf{X} + \mathbf{B}_n\,\mathbf{U} + \mathbf{W}_n + \mathbf{D} \tag{18}$$

For the system Eq. (18), we define the sliding surface as the tracking error by [26]

$$\mathbf{S} = \mathbf{X} - \mathbf{X}_{ref} \tag{19}$$

Combining Eqs. (18) and (20) and assuming that $\mathbf{X}_{ref}$ is differentiable, $\dot{\mathbf{S}}$ is given by

$$\dot{\mathbf{S}} = \mathbf{A}_n\,\mathbf{X} + \mathbf{B}_n\,\mathbf{U} + \mathbf{W}_n + \mathbf{D} - \dot{\mathbf{X}}_{ref} \tag{20}$$

To bring out an error term, the term $\mathbf{A}_n\,\mathbf{X}_{ref}$ can be added and subtracted to the above equation, which leads to

$$\dot{\mathbf{S}} = \mathbf{A}\,\mathbf{S} + \left(\mathbf{B}_n\,\mathbf{U} + \mathbf{W}_n + \mathbf{D} + \mathbf{A}_n\,\mathbf{X}_{ref} - \dot{\mathbf{X}}_{ref}\right) \tag{21}$$

Now a control action $\mathbf{U}$ can be chosen such that the term between brackets in Eq. (21) is zero at any instant of time [23]. This makes the error decay at the rate dictated by the state matrix $\mathbf{A}_n$. Since this decay rate is not practical in general, a much faster one is desired. Thus a new control action

$$\mu = \mathbf{U} + \mathbf{K}\,\mathbf{S} \tag{22}$$

is defined to adjust the error dynamics, where $\mathbf{K}$ is a feedback gain matrix [23]. The error dynamics now takes the form

$$\dot{\mathbf{S}} = (\mathbf{A}_n - \mathbf{B}_n\,\mathbf{K})\,\mathbf{S} + \mathbf{p}, \tag{23}$$

where vector $\mathbf{p}$ is expressed as follows:

$$\mathbf{p} = \mathbf{B}_n \mu + \mathbf{W}_n + \mathbf{A}_n \mathbf{X}_{ref} - \dot{\mathbf{X}}_{ref} + \mathbf{D} \tag{24}$$

The proposed control law is chosen as follows:

$$\mu = \mathbf{B}_n^{-1} \left(-\mathbf{W}_n - \mathbf{A}_n \mathbf{X}_{ref} + \dot{\mathbf{X}}_{ref} - \hat{\mathbf{D}} - \mathbf{L}\,\mathbf{sign}(\mathbf{S}) \right), \tag{25}$$

where $\hat{\mathbf{D}}$ is the estimated of $\mathbf{D}$.$\mathbf{L}$ and $\mathbf{sign}(\mathbf{S})$ are given as follows:

$$\mathbf{L} = \mathbf{diag}\begin{pmatrix} l_1 & l_2 & l_3 & l_4 \end{pmatrix}, \quad l_i > 0 \text{ for } i = 1, ..., 4 \text{ and}$$

$$\mathbf{sign}(\mathbf{S}) = [sign(s_1)\ sign(s_2)\ sign(s_3)\ sign(s_4)]^T.$$

Here $x \mapsto sign(x)$ refers to the sign function.

The error dynamic behavior in the time interval $[t-L, t]$, where L is a delay time, is governed by Eq. (23) and its response at present time t is given as follows [23]:

$$\mathbf{S}(t) = \Phi(t, t-L)\,\mathbf{S}(t-L) + \int_{t-L}^{t} \Phi(t-\tau, t-L)\,\mathbf{p}(\tau)\,d\tau, \tag{26}$$

which involves a state transition matrix Φ expressed as [22]

$$\Phi(t_1, t_2) = \mathbf{e}^{(\mathbf{A}_n - \mathbf{B}_n \mathbf{K})(t_1 - t_2)} \tag{27}$$

If $\mathbf{A}_n$, $\mathbf{B}_n$, $\mathbf{W}_n$, μ, $\mathbf{S}$, $\mathbf{X}_{ref}$, $\dot{\mathbf{X}}_{ref}$, and $\mathbf{K}$ are specified along the time interval $[t-L,\ t]$, the unknown function $\mathbf{D}(t)$ can be estimated through rearranging Eq. (26) as

$$\begin{aligned} \int_{t-L}^{t} \Phi(t-\tau,\, t-L)\,\mathbf{D}(\tau)\,d\tau &= \mathbf{S}(t) - \Phi(t, t-L)\,\mathbf{S}(t-L) \\ - \int_{t-L}^{t} \Phi(t-\tau,\, t-L) &\left(\mathbf{B}_n \mu + \mathbf{W}_n + \mathbf{A}_n \mathbf{X}_{ref} - \dot{\mathbf{X}}_{ref} \right) d\tau \end{aligned} \tag{28}$$

For a small time delay L, $\mathbf{D}(t)$ does not change significantly during the time interval $[t-L,\ t]$, and so it can be approximated by $\hat{\mathbf{D}}(t)$ as follows [23]:

$$\int_{t-L}^{t} \Phi(t-\tau\,,\, t-L)\,\mathbf{D}(\tau)\,d\tau = \left(\int_{t-L}^{t} \Phi(t-\tau\,,\, t-L)\,d\tau \right) \hat{\mathbf{D}}(t) \tag{29}$$

and thus

$$\hat{\mathbf{D}}(t) = \left(\int_{t-L}^{t} \Phi(t-\tau\,,\, t-L)\,d\tau \right)^{-1} \int_{t-L}^{t} \Phi(t-\tau\,,\, t-L)\,\mathbf{D}(\tau)\,d\tau \tag{30}$$

Once the unknown vector $\mathbf{D}(t)$ is estimated, the control action can be calculated by Eq. (25) as in [23–25].

Note that the proposed control law, when implemented digitally, suggests a delay time L much larger than the sampling period T [23].

As the time delay L is small enough but not zero, it is assumed that the estimated vector $\hat{\mathbf{D}}(t)$ at present time is closer to the value of $\mathbf{D}(t)$ and so an estimation error εcould exist.

$$\varepsilon = \mathbf{D}(t) - \hat{\mathbf{D}}(t) \tag{31}$$

However, it is reasonable to assume that the approximation error is bounded [23–25]. Hence, there exist four positive constants $\bar{\varepsilon}_i$ such that

$$|\varepsilon_i| \leq \bar{\varepsilon}_i, i = 1, ..., 4 \tag{32}$$

Theorem *If the control law defined by Eq. (25) with the estimation law Eq. (30) are applied to the VSC-HVDC system described by Eq. (18) under the condition Eq. (32) and properly chosen design matrices* $\mathbf{K}$ *and* $\mathbf{L}$*, then the following important properties can be guaranteed:*

1. *all signals in the closed-loop system remain bounded,*
2. *the tracking error* $\mathbf{S}(t)$ *converges to zero in a finite time given by Eq. (43).*

Proof The Lyapunov function candidate, which must be positive definite and radially unbounded, is chosen as follows:

$$V = \frac{1}{2} \sum_{i=1}^{4} s_i^2 = \frac{1}{2} \mathbf{S}^T \mathbf{S} \tag{33}$$

Using Eqs. (23), (24), and (31) and replacing μ by its expression Eq. (25), one obtains the time derivative of $\mathbf{S}$ as follows:

$$\begin{aligned} \dot{\mathbf{S}} &= (\mathbf{A}_n - \mathbf{B}_n \mathbf{K}) \mathbf{S} + \left(\mathbf{D} - \hat{\mathbf{D}} - \mathbf{L}\,\mathbf{sign}(\mathbf{S})\right) \\ &= (\mathbf{A}_n - \mathbf{B}_n \mathbf{K}) \mathbf{S} + (\varepsilon - \mathbf{L}\,\mathbf{sign}(\mathbf{S})) \end{aligned} \tag{34}$$

Thus, the time derivative of V is given as follows:

$$\dot{V} = \mathbf{S}^T \dot{\mathbf{S}} = \mathbf{S}^T (\mathbf{A}_n - \mathbf{B}_n \mathbf{K}) \mathbf{S} + \mathbf{S}^T (\varepsilon - \mathbf{L}\,\mathbf{sign}(\mathbf{S})) \tag{35}$$

It is worth noting that the matrix $\mathbf{K}$ should be calculated by pole assignment method so as all eigenvalues of the matrix $\mathbf{A}_n - \mathbf{B}_n \mathbf{K}$ have real parts negative. In this case, the term $\mathbf{S}^T (\mathbf{A}_n - \mathbf{B}_n \mathbf{K}) \mathbf{S}$ is negative; thus Eq. (35) gives the right to write:

$$\dot{V} \leq \mathbf{S}^T (\varepsilon - \mathbf{L}\,\mathbf{sign}(\mathbf{S})) \tag{36}$$

The inequality Eq. (36) can be rewritten as

$$\dot{V} \leq \sum_{i=1}^{4} (s_i \varepsilon_i - l_i |s_i|) \tag{37}$$

If the following condition $l_i \geq \bar{\varepsilon}_i$ holds then $\dot{V}$ will be negative definite. Indeed,

$$\dot{V} \leq -\alpha \sum_{i=1}^{4} |s_i|, \tag{38}$$

where $\alpha = \min_{i=1 \cdots 4} \{l_i - \bar{\varepsilon}_i\}$ is a positive constant. □

Therefore, $\mathbf{S}(t)$ converges asymptotically to zero and all signals are bounded. This means that by a suitable choice of state feedback matrix gain $\mathbf{K}$ and switching matrix $\mathbf{L}$, control objectives will be achieved (i.e. $\lim_{t\to\infty} \mathbf{S}(t) = 0$, then $\lim_{t\to\infty} \mathbf{X}(t) = \mathbf{X}_{ref}$).

Using Eqs. (38) and (33) and the fact that $\sqrt{\sum_{i=1}^{4} s_i^2} \leq \sum_{i=1}^{4} |s_i|$, one can write

$$\dot{V} \leq -\sqrt{2}\,\alpha\,\sqrt{V} \tag{39}$$

Multiplying inequality Eq. (39) by $\frac{dt}{2\sqrt{V}}$, replacing $\dot{V}$ by $\frac{dV}{dt}$ and integrating both sides of resulting inequality over the interval $[0\,;\ t]$ yields

$$\int_{V(0)}^{V(t)} \frac{dV}{2\sqrt{V}} \leq -\frac{\alpha}{\sqrt{2}} \int_{0}^{t} dt \tag{40}$$

Thus

$$\sqrt{V(t)} - \sqrt{V(0)} \leq -\frac{\alpha}{\sqrt{2}}\,t \tag{41}$$

Since $V(t)$ is a decreasing function (i.e. $\sqrt{V(0)} \geq \sqrt{V(t)}$), Eq. (41) conducts to

$$\frac{\alpha}{\sqrt{2}}\,t \leq \sqrt{V(0)} \tag{42}$$

Eq. (42) implies that $\mathbf{S}(t)$ converges to zero in finite time and reaches this value at most after $\bar{t}$ units of time.

$$\bar{t} = \frac{\sqrt{2}}{\alpha}\sqrt{V(0)} \tag{43}$$

Hence, the proof is achieved completely.

According to Eq. (43), a large α results in a shorter time $\bar{t}$. Hence, the designer should select matrices $\mathbf{L}$ and $\mathbf{K}$ in accordance with the convergence time $\bar{t}$ to be small and the control input μ not being very large in terms of energy. Once the control vector μ is obtained, the real control action can be calculated using Eqs. (22) and (25).

$$\mathbf{U} = \mathbf{B}_n^{-1}\left(-\mathbf{W}_n - \mathbf{A}_n\,\mathbf{X}_{ref} + \dot{\mathbf{X}}_{ref} - \hat{\mathbf{D}} - \mathbf{L}\,\mathbf{sign}(\mathbf{S})\right) - \mathbf{K}\,\mathbf{S} \tag{44}$$

To show the effectiveness and superiority of the proposed ASMTDCC technique, its performances should be compared to those of conventional sliding mode control (SMC) as proposed in [16,17]. Likewise, to ensure stability while designing the SMC controller, an appropriate positive definite Lyapunov energy function candidate as Eq. (33) $V = \frac{1}{2}\,\mathbf{S}^T\,\mathbf{S} > 0$ is chosen; thus $\dot{V} = \mathbf{S}^T\,\dot{\mathbf{S}}$. To ensure that $\dot{V} < 0$, $\dot{\mathbf{S}}$ is selected among the set of formula listed in [16,17] with mandatory positive definite tuning matrix gains $\mathbf{K_1}$ (switching gain) and $\mathbf{K_2}$ (vanishing gain). If $\dot{\mathbf{S}} = -\mathbf{K_1}\,\mathbf{sign}(\mathbf{S}) - \mathbf{K_2}\,\mathbf{S}$ then in its centralized form and considering nominal model the SMC law can be given as follows [16]:

$$\mathbf{U} = \mathbf{B}_n^{-1}\left(-\mathbf{W}_n - \mathbf{A}_n\,\mathbf{X}_{ref} + \dot{\mathbf{X}}_{ref} - \mathbf{K_1}\,\mathbf{sign}(\mathbf{S}) - \mathbf{K_2}\,\mathbf{S}\right) \tag{45}$$

The main difference between the two controllers based on sliding modes is that the ASMTDCC includes the estimation lumped disturbance $\hat{\mathbf{D}}$, which cancels the lumped plant uncertainties and disturbances $\mathbf{D}$ with relatively low gains, while the SMC uses only tuned gains, which should be relatively higher, to realize the disturbance rejection.

5. Simulation and discussion

In this section, the performances of the proposed control scheme, in terms of response to power flow variation and DC voltage regulation, are illustrated by numerical simulations given in Figures 7–9, for a 4-min run. The performance of the presented controller is compared with that of the conventional SMC controller with the following parameters [16,17]: $\mathbf{K_1} = 10^2 \times$ blockdiag (1.5 1.5 1.5 1.5) and $\mathbf{K_2} = 10^3 \times$ blockdiag (1.5 1.5 1.5 1.5).

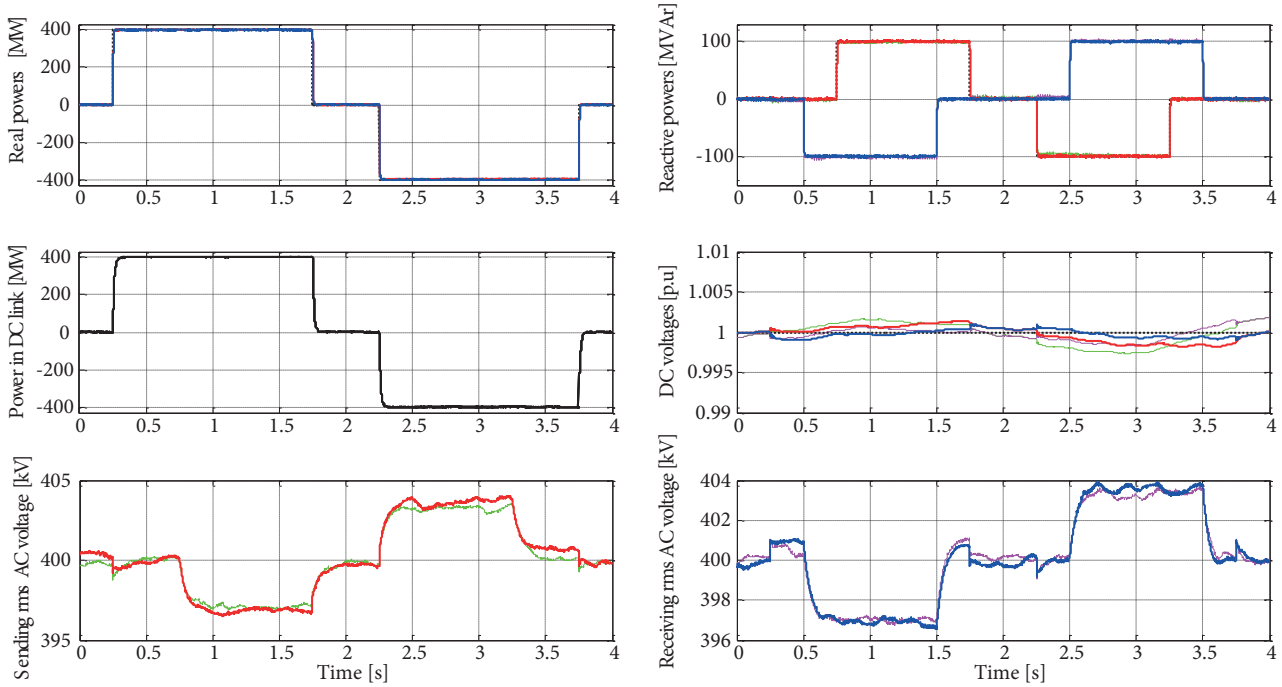

Figure 7. System responses without uncertainties (test 1).

For ASMTDCC, dashed black, solid red, and solid blue thick lines refer to references, sending side, and receiving side responses, respectively. For the SMC controller, solid green and solid magenta thin lines refer to sending side and receiving side responses, respectively.

Meanwhile, the proposed controller has been tested in three cases: nominal operation without uncertainties (test 1), operation considering parameter variations (test 2), and operation under external disturbances (test 3).

The parameter values used to simulate the VSC-HVDC model are selected as follows:

Voltage base $V_b = 400\,kV\,rms$, Power base $S_b = 1000\,MVA$,

Source voltages: $V_s = V_r = 1\,p.u$, AC lines: $Z_s = Z_r = 0.001 + 0.012\,p.u$,

DC line: $Z_{dc} = 0.05 + 0.10\,p.u, 1/(C_1\,\omega_1) = 1/(C_2\,\omega_2) = 0.15\,p.u$

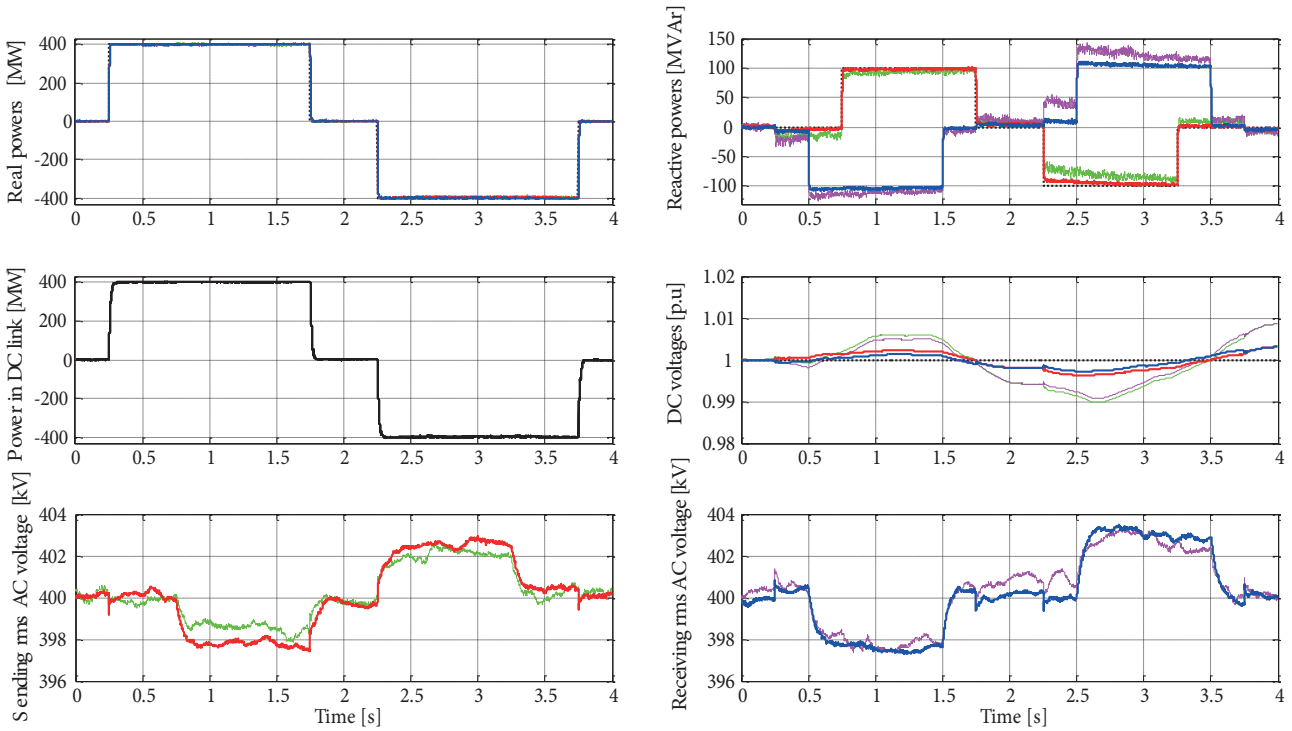

Figure 8. System responses with 30% of parameter uncertainties (test 2).

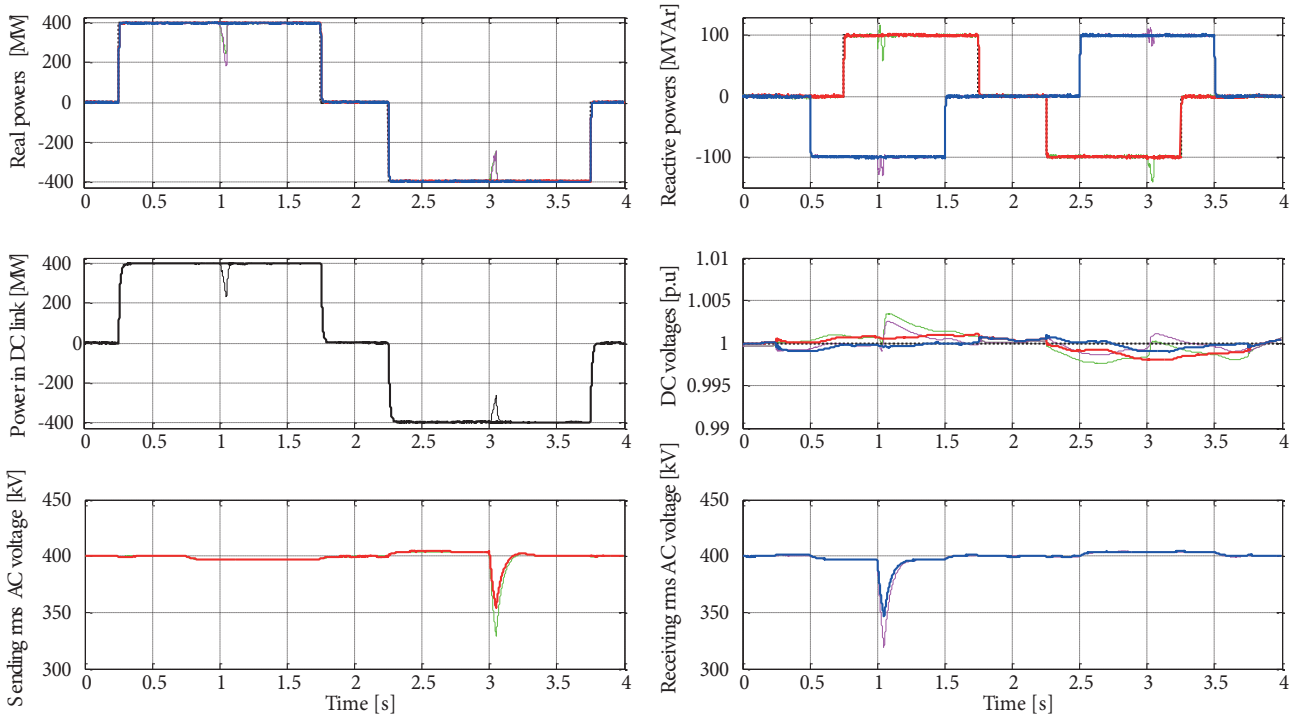

Figure 9. System responses with 30% voltage drops (test 3).

Note that all the design parameters in the ASMTDCC systems are chosen to achieve a satisfactory transient control performance considering the requirement of stability. $\mathbf{L} = 10^2 \times \text{blockdiag} \quad (2.3 \quad 1.1 \quad 2.1 \quad 0.9)$, dominant poles of $\mathbf{A}_n - \mathbf{B}_n \mathbf{K}$ are $p_{1,2} = -248 \pm j\,253$.

For outer loop DC voltage PI controller, the parameters are $k_p = 10$ and $k_i = 75$.

The simulation results of the control scheme with the proposed ASMTDCC method are depicted in Figures 7–9, which show clearly that the proposed controller works well. Indeed, one can see that the proposed controller has diminished the interaction between active and reactive powers and that the DC-link voltages are controlled to their standard boundary. Moreover, it is obvious that the speed of the response and transient conditions are further improved in comparison with the conventional SMC controller, whose responses are dependent on model uncertainties, external disturbances, and reference variations. The proposed controller seems to be robust against parameter variations and insensitive to external disturbances. In addition, the proposed controller ensures chattering-free control by selecting switching gains sufficiently small in comparison with those of traditional sliding mode control as in [16,17].

It is also shown that in disturbed case in Figures 8 and 9, the performances of the system controlled by the proposed ASMTDCC, with finite time convergence, are significantly better than those obtained by the conventional SMC controller, with asymptotic convergence.

6. Conclusion

In this paper, a robust ASMTDCC is developed for power flow control of a power system based on the VSC-HVDC transmission system. The model of VSC-HVDC transmission system, which has been developed in state space, is linear; however, it is assumed that the system is perturbed by inherent uncertainty and external disturbances. Based on time delay estimation with convolution, the unknown disturbance term of equivalent control in the AC subsystem can be estimated and relaxes thereby the usual dynamics modeling requirement. The designed controller is able to stabilize the error trajectories of the system to origin in a given finite time rather than infinite horizon. The finite time stability, robustness, and disturbance rejection of the proposed controller are mathematically proved. Numerical simulations validate the theoretical results using an asynchronous two-bus test system. Simulation results show the superiority of the VSC-HVDC transmission system equipped with the proposed controller over the conventional SMC controller in convergence time and robustness.

References

[1] Woodford DA. HVDC Transmission. Manitoba HVDC Research Centre, Manitoba, Canada, 1998.

[2] Aredes M, Aquino A, Santos G. Multipulse converters and controls for HVDC and FACTS systems. Electr Eng 2001; 83: 137-145.

[3] Moustafa M, Filizadeh S. HVDC model with reduced computational intensity. In: IEEE 2012 Power and Energy Society General Meeting; 22–26 July 2012; San Diego, CA, USA: IEEE. pp. 1-6.

[4] Rudervall R, Charpentier J, Sharma R. High Voltage Direct Current (HVDC) Transmission Systems Technology Review Paper. In: Energy Week 2000; March 7–8; Washington, DC, USA: 1-17.

[5] Ahmed M, Ebrahim M, Ramadan H, Becherif M. Optimal genetic-sliding mode control of VSC-HVDC transmission systems. In: Energy Procedia 2015 International Conference on Technologies and Materials for Renewable Energy, Environment and Sustainability, TMREES15 2015; April 17–20; Beirut, Lebanon 74: 1048-1060.

[6] Ayan K, Kılıç U. Optimal power flow of two-terminal HVDC systems using backtracking search algorithm. Int J Elec Power 2015; 78: 326-335.

[7] Carrizosa M, Navas F, Damm G, Lagarrigue F. Optimal power flow in multi-terminal HVDC grids with offshore wind farms and storage devices. Int J Elec Power 2015; 65: 291-298.

[8] Castro L, Acha E, Esquivel E. A novel VSC-HVDC link model for dynamic power system simulations. Electr Pow Syst Res 2015; 126: 111-120.

[9] Chen Y, Dai J, Damm G, Lagarrigue F. Small Signal Stability Analysis of Power System Equipped with VSC based Back to Back HVDC. In: IEEE 2015 2nd Int'l Conf. on Electrical Engineering and Information & Communication Technology (ICEEICT) 2015; 21–23 May 2015; Jahangirnagar University, Dhaka-1342, Bangladesh. USA: IEEE. pp. 1-6.

[10] Nnachi AF, Munda J, Nicolae DV, Mpanda AM. Transient stability analysis of VSC HVDC transmission with power injection on the DC-link. Turk J Elec Eng & Comp Sci 2015; 23: 1834-1852.

[11] Ruan S, Li G, Peng L, Sun Y, Lie T. A nonlinear control for enhancing HVDC light transmission system stability. Int J Elec Power 2007; 29: 565-570.

[12] Bidadfar A, Abedi M, Karrari M, Gharehpetian G, Tavana S. Passive AC network supplying the integration of CCC-HVDC and VSC-HVDC systems. Turk J Elec Eng & Comp Sci 2014; 22: 353-362.

[13] Guo C, Zhao C. A New Technology for HVDC Start-up and Operation Using VSC-HVDC System. In: IEEE 2009 Power and Energy Society General Meeting PES'09; 26-30 July 2009; Calgary, Alberta Canada, USA: IEEE. pp. 1-5.

[14] Mazouz L, Zidi S, Khatir M, Benmessaoud T, Saadi S. Particle swarm optimization based PI controller of VSC-HVDC system connected to a wind farm. Int J Syst Assur Eng Manag 2015; 1-8.

[15] Liang H, Li G, Li G, Li P, Yin M. Analysis and Design of H∞ Controller in VSC-HVDC Systems. In: IEEE 2005 Transmission and Distribution Conference & Exhibition; 14–18 August 2005; Asia and Pacific Dalian, China, USA: IEEE. pp. 1-6.

[16] Ramadan H, Siguerdidjane H, Petit M, Kaczmarek R. Performance enhancement and robustness assessment of VSC-HVDC transmission systems controllers under uncertainties. Int J Elec Power 2012; 35: 34-46.

[17] Ramadan H, Siguerdidjane H, Petit M. A Robust Stabilizing Nonlinear Control Design for VSC-HVDC Systems: A Comparative Study. In: IEEE 2009 International Conference on Industrial Technology; 10–13 February 2009; Gippsland, Australia, USA: IEEE. pp. 1-6.

[18] Chen Y, Dai J, Damm G, Lagarrigue F. Nonlinear control design for a multi-terminal VSC-HVDC system. In: IEEE 2013 12th European Control Conference (ECC 2013); Jul 2013; Zurich, Switzerland, USA: IEEE. pp. 3536-3541.

[19] Ruan S, Li G, Jiao X, Sun Y, Lie T. Adaptive control design for VSC-HVDC systems based on backstepping method. Electr Pow Syst Res 2007; 77: 559-565.

[20] Rigatos G, Siano P, Wira P, Cecati C. A Global Linearization Approach to Control and State Estimation of a Voltage Source Converter: HVDC System. Intell Ind Syst 2015; 1: 331-344.

[21] Lee T. Lagrangian modeling and passivity-based control of three-phase AC/DC voltage-source converters. IEEE T Ind Electron 2004; 51: 892-902.

[22] Liu Y, Li R. A novel control method for a VSC-HVDC system in a grid-connected wind farm. Turk J Elec Eng & Comp Sci 2015; 23: 1558-1570.

[23] Youcef-Toumi K, Huang S. Analysis of a Time Delay Controller Based on Convolutions. In: IEEE 1993 Proceeding of the American Control Conference (ACC 1993); 2–4 June; San Francisco, California, USA: IEEE. pp. 2582 -2586.

[24] Wang Y, Yu D, Kim Y. Robust time-delay control for the DC-DC boost converter. IEEE T Ind Electron 2014; 61: 4829-4837.

[25] Lee S, Chang P. The development of anti-windup scheme for time delay control with switching action using integral sliding surface. J Dyn Syst-T ASME 2013; 125: 630-638.

[26] Köse E, Kizmaz H, Abaci K, Aksoy S. Control of SVC based on the sliding mode control method. Turk J Elec Eng & Comp Sci 2014; 22: 605-619.